

Prediction of perforation velocity of hard missile impacts on reinforced concrete wall panels

Andac Lulec, Vahid Sadeghian, and Frank J. Vecchio

Abstract: This study reviews and compares the most commonly used models for computing the local effects of hard missile impacts. The accuracies of the models in predicting perforation velocity are evaluated using a dataset of 95 impact tests collected from the literature. It is found that the majority of the models are unable to accurately predict perforation velocity or have a limited application range because of their empirical nature. To address these limitations, a semi-analytical model based on the Modified Compression Field Theory and the principle of work and energy is proposed. Unlike most existing models, the proposed model is capable of considering the influence of in-plane and shear reinforcement. The performance of the proposed model is assessed against experimental results obtained from the compiled dataset as well as other existing models.

Key words: reinforced concrete panels, impact loading, hard missile, perforation, analytical model.

Résumé : Cette étude examine et compare les modèles les plus couramment utilisés pour calculer les effets locaux des impacts de missiles durs. L'exactitude des modèles de prévision de la vitesse de perforation est évaluée à l'aide d'un ensemble de données de 95 essais d'impact recueillis dans la littérature. On constate que la majorité des modèles sont incapables de prédire avec précision la vitesse de perforation ou ont une portée d'application limitée en raison de leur nature empirique. Pour remédier à ces limitations, un modèle semi-analytique fondé sur la théorie des champs de compression modifiée et le principe du travail et de l'énergie est proposé. Contrairement à la plupart des modèles existants, le modèle proposé peut tenir compte de l'effet de renforcement dans le plan et de cisaillement. Le rendement du modèle proposé est évalué en fonction des résultats expérimentaux obtenus à partir de l'ensemble de données compilées et d'autres modèles existants. [Traduit par la Rédaction]

Mots-clés : éléments en béton armé, charges d'impact, missile dur, perforation, modèle analytique.

1. Introduction

The behaviour of reinforced concrete (RC) structures under impact has been the subject of many research studies. Interest in this research topic was initially triggered by military-related concerns; it later extended to many other applications including the design of buildings, bridges, offshore platforms, and nuclear power plants subjected to accidental or intentional impact loading scenarios (e.g., falling rock, terrorist attack, vehicle or ship collision).

In general, missile impacts can be classified into two groups according to the missile rigidity: soft and hard missile impacts. In a soft missile impact, the missile deformation is significant and the overall behaviour of the target is typically flexural and global in nature without considerable local deformation. In contrast, under a hard missile impact, the missile deformation is negligible compared to that of the target and damage is significantly localized in the vicinity of the impact region. Although significant efforts have been made to study the local effects caused by hard missile impacts, these effects are still not fully understood and additional work is needed.

Depending on the velocity of a hard missile impact, the local deformations and damage mechanisms inflicted on the target can vary significantly. Missiles with low velocities rebound from

the target creating little or no local damage. With increasing velocities, the missile causes surface damage typically in the form of a spalling crater on the front face of the target. As the velocity increases further, the missile penetration depth increases and eventually cracking appears at the back of the target followed by scabbing of the concrete. Finally, with higher velocities, the missile perforates the target with a residual velocity. These local deformation conditions are demonstrated in Fig. 1.

Empirical models are typically used to calculate important parameters required in designing RC structures against impact. These parameters are the penetration depth of missiles, the minimum target thickness required to prevent scabbing (i.e., scabbing thickness) or perforation (i.e., perforation thickness), and the minimum missile velocity required to cause perforation (i.e., perforation velocity). Despite their common use, existing models have two major limitations. First, majority of the models are based on empirical relations which limit their validity to the range of data used for their calibration. Second, most of the models do not consider the influence of in-plane reinforcement or shear reinforcement. Thus, the applicability of these models becomes questionable for modern structures having in-plane and shear reinforcement.

This study aims to use the existing experimental data and well-recognized theoretical concepts to further examine the

Received 28 August 2019. Accepted 29 December 2019.

A. Lulec* and F.J. Vecchio. Department of Civil and Mineral Engineering, University of Toronto, Toronto, ON, Canada.

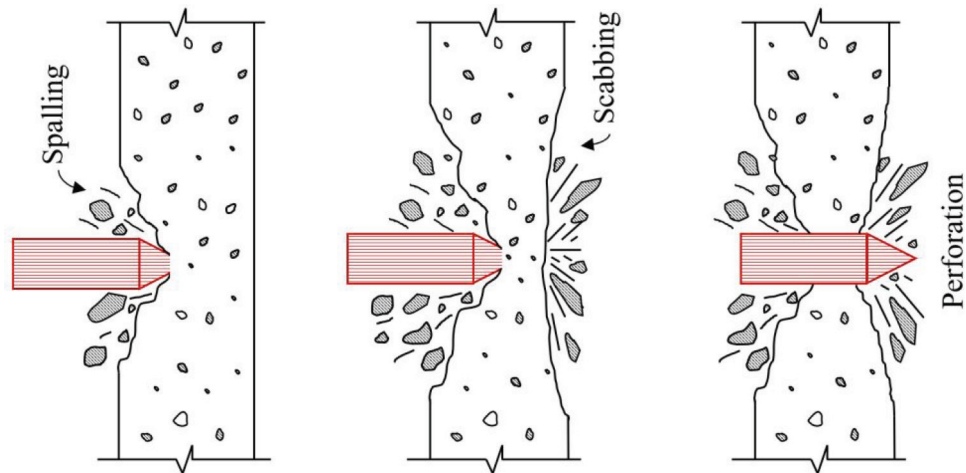
V. Sadeghian. Department of Civil and Environmental Engineering, Carleton University, Ottawa, ON, Canada.

Corresponding author: Vahid Sadeghian (email: vahid.sadeghian@carleton.ca).

*Current affiliation: BBA Consulting Engineering, Toronto, ON, Canada.

Copyright remains with the author(s) or their institution(s). Permission for reuse (free in most cases) can be obtained from copyright.com.

Fig. 1. Local deformations under a hard missile impact. [Colour online.]



behaviour of RC panels subjected to hard missile impacts. First, the performance of existing models in predicting local effects of hard missiles is evaluated using a dataset of 95 impact tests collected from the literature. Then, a semi-analytical model is proposed for the prediction of perforation velocity that takes into account the effects of both in-plane and shear reinforcement. Finally, the accuracy of the model is compared against a wide range of impact tests as well as against the commonly used models found in the literature.

2. Review of existing models

Most of the existing models for predicting the local effects of hard missile impacts were developed based on regression analysis of data reported from tests conducted prior to 1950s. The missiles and targets used in these tests were typically highly rigid and nondeformable; the missile was often a projectile or bomb casing made of steel, while the target was a thick concrete slab. Because of the high rigidity of the missiles and targets, it is expected that existing models overestimate local effects, especially when there is noticeable deformation in the missiles or targets (Kennedy 1976). Additionally, the ranges of the parameters used for these tests were limited, which raises concern about the applicability of empirical models to other types of structural elements. This concern becomes more significant when one considers the changes made in the design and construction process of RC walls and slabs over the last several decades.

In the following, 13 commonly used models in the literature are reviewed and compared. Table 1 summarizes the equations that each model employs to calculate the penetration depth, scabbing thickness, and perforation velocity. It can be seen that some models cannot compute one or two of these parameters. Table 1 also presents the applicability range of each model. While some models have no limitations in terms of application range, others are only applicable to a narrow range of test parameters. The description and units of the terms used in Table 1 are presented in Table 2 and throughout this section.

One of the oldest and most commonly used models is the Modified Petry model originally developed for military purposes in 1910 (Samuely and Hamann 1939). The model is based on the equation of motion in which the resistance force is expressed as a function of the missile initial velocity (V), the weight per unit projected area of the missile (A_p), and a constant describing the penetrability of concrete (K). The original model does not consider the influence of the concrete and reinforcement properties

of the target. In the modified model, the concrete penetrability factor varies depending on the level of in-plane reinforcement. Later, Amirikian (1950) proposed a more refined expression for K , which also accounts for the concrete strength.

Another widely used model is a set of relations proposed by the Army Corps of Engineers (ACE) based on statistical fitting to data obtained from a large experimental campaign carried out by the Ordnance Department of the US Army and the Ballistic Research Laboratory (BRL) in 1940s (ACE 1946). These tests were mostly performed on thick concrete specimens subjected to high-velocity missiles with large diameters. Thus, the ACE model is more suitable for large structural systems such as nuclear power plants.

Based on findings obtained from the ACE model, the National Defense Research Committee (NDRC) developed a theory to calculate the penetration of rigid missiles into massive concrete targets (NDRC 1946). In addition to the final penetration depth, this theory can also be used to calculate the variation of the impact force and the penetration depth during the impact. To consider the influence of missile shape on the penetration depth, a missile shape factor (N) was defined in the model. Chelapati et al. (1972) extended the NDRC model and suggested formulae for calculating the scabbing and perforation thicknesses by curve fitting to experimental data. Because of its semi-theoretical basis, the NDRC model has a wider application range compared to the ACE model.

Over the years, the NDRC model has been used as the basis for many other models. Kar (1978) proposed a modified version of the NDRC model applicable to missiles made of various materials. In this model, the missile local effects are a function of the ratio of the modulus of elasticity of the missile (E) to the modulus of elasticity of the mild steel (E_m). Also, to the best of the authors' knowledge, this is the only model that considers the effect of concrete aggregate size ($2a$) on the scabbing and perforation thickness. Based on a statistical analysis of test data, Degen (1980) proposed a new formula for perforation thickness in which the penetration depth was estimated according to the NDRC model. Haldar and Miller (1982) suggested another model to predict the penetration depth, which uses similar parameters as those used in the NDRC model. Later, Haldar and Hamieh (1984) used regression analysis of test data to extend this model and estimate the scabbing thickness.

Hughes (1984) proposed a new model to calculate the local effects of a hard missile impact. The model is able to consider the loading rate effects on the tensile strength of concrete using a

Table 1. Summary of commonly used models for predicting local effects of a hard missile impact.

Model	Penetration depth (X_p)	Scabbing thickness (d_s)	Perforation thickness (d_p)	Application range
Petry	(1) $X_p = 12K_p A_p \log_{10} \left(1 + \frac{V^2}{19974} \right)$	(2) $d_s = 2.2X_p$	(3) $d_p = 2X_p$	Without limitation.
ACE	(4) $\frac{X_p}{D} = \frac{0.00019W}{D^{2.785} f_c^{0.5}} \left(\frac{V}{304.8} \right)^{1.5} + 0.5$	(5) $\frac{d_s}{D} = 2.12 + 1.36 \frac{X_p}{D}$	(6) $\frac{d_p}{D} = 1.32 + 1.24 \frac{X_p}{D}$	eq. 5 $0.65 \leq \frac{X_p}{D} \leq 11.75$ eq. 6 $1.35 \leq \frac{X_p}{D} \leq 13.50$
NDRC	(7) $\begin{cases} \frac{X_p}{D} = \sqrt{\frac{\lambda}{32553}} & \frac{X_p}{D} \leq 2.0 \\ \frac{X_p}{D} = 1 + \frac{\lambda}{130212} & \frac{X_p}{D} > 2.0 \end{cases}$	(10) $\frac{d_s}{D} = 7.91 \frac{X_p}{D} - 5.06 \left(\frac{X_p}{D} \right)^2$	(11) $\frac{d_p}{D} = 3.19 \frac{X_p}{D} - 0.718 \left(\frac{X_p}{D} \right)^2$	eq. 10 $\frac{X_p}{D} \leq 0.65$ eq. 11 $\frac{X_p}{D} \leq 1.35$ For larger $\frac{X_p}{D}$ use eqs. 5 and 6
	(8) $\lambda = \frac{KNW}{D^{2.8}} \left(\frac{V}{304.8} \right)^{1.8}$			
	(9) $K = \frac{14.95}{\sqrt{f_c}}$			
BRL	N/A	(12) $d_s = 2d_p$	(13) $\frac{d_p}{D} = \frac{2.723 \times 10^{-4} W}{D^{2.8} f_c^{0.5}} \left(\frac{V}{304.8} \right)^{1.33}$	Without limitation
Bechtel	N/A	(14) $d_s = 1.564 \times 10^{-2} \frac{W^{0.4} V^{0.5}}{D^{0.2} f_c^{0.5}}$	N/A	Without limitation
CEA-EDF	N/A	N/A	(15) $d_p = \frac{4.609 \times 10^{-3} m^{0.5} V^{0.75}}{\rho^{0.125} D^{0.5} f_c^{0.375}}$	$20 < V < 200$ $0.3 < \frac{d_p}{D} < 4.0$ $30 < f_c' < 45$ $75 < r < 300$
CEA-EDF (r)	N/A	N/A	(16) $d_p = (d_{p, \text{CEA}}) \left(\frac{750}{500 + r} \right)^{0.75}$	Similar to the CEA-EDF model with minor changes

Table 1 (continued).

Model	Penetration depth (X_p)	Scabbing thickness (d_s)	Perforation thickness (d_p)	Application range
Chang	N/A	(17) $d_s = \frac{7.325 \times 10^{-3} \lambda^{0.13} (m V^2)^{0.4}}{D^{0.2} f_c^{0.4}}$	(19) $d_p = 0.001 \lambda^{0.25} \left(\frac{m V^2}{D f_c} \right)^{0.5}$	16.7 < V < 311.8 22.8 < f_c' < 45.5 0.11 < m < 344 0.020 < D < 0.305
		(18) $\lambda = \left(\frac{61}{V} \right)$		
Degen	Same as the NDRC model.	N/A	(20), (21) $\begin{cases} \frac{d_p}{D} = 0.69 + 1.29 \frac{X_p}{D} \\ \frac{d_p}{D} = 2.2 \frac{X_p}{D} - 0.3 \left(\frac{X_p}{D} \right)^2 \end{cases}$	eq. 20 $1.52 \leq \frac{X_p}{D} \leq 13.4$ eq. 21 $\frac{X_p}{D} \leq 1.52$ 25 < V < 312 28 < f_c' < 43 0.15 < d_p < 0.61 0.1 < D < 0.31
Kar	(22), (23) $\begin{cases} \frac{X_p}{D} = \sqrt{\frac{\lambda}{32553}} & \frac{X_p}{D} \leq 2.0 \\ \frac{X_p}{D} = 1 + \frac{\lambda}{130212} & \frac{X_p}{D} > 2.0 \end{cases}$	(25), (26) $\begin{cases} \lambda = 7.91 \frac{X_p}{D} - 5.06 \left(\frac{X_p}{D} \right)^2 \\ \lambda = 2.12 + 1.36 \frac{X_p}{D} \end{cases}$	(28), (29) $\begin{cases} \lambda = 3.19 \frac{X_p}{D} - 0.718 \left(\frac{X_p}{D} \right)^2 \\ \lambda = 1.32 + 1.24 \frac{X_p}{D} \end{cases}$	eq. 25 $\frac{X_p}{D} \leq 0.65$ eq. 26 $0.65 \leq \frac{X_p}{D} \leq 11.75$ eq. 28 $\frac{X_p}{D} \leq 1.35$ eq. 29 $1.35 \leq \frac{X_p}{D} \leq 13.5$
	(24) $\lambda = \frac{KNW}{D^{2.8}} \left(\frac{E}{E_m} \right)^{1.25} \left(\frac{V}{304.8} \right)^{1.8}$	(27) $\lambda = \frac{d_s - a}{D} \left(\frac{E_m}{E} \right)^{0.2}$	(30) $\lambda = \frac{d_p - a}{D} \left(\frac{E_m}{E} \right)^{0.2}$	
Haldar	(31), (32), (33) $\begin{cases} \frac{X_p}{D} = -0.02725 + 0.22024(\lambda) \\ \frac{X_p}{D} = -0.592 + 0.446(\lambda) \\ \frac{X_p}{D} = 0.53886 + 0.06892(\lambda) \end{cases}$	(35) $\frac{d_s}{D} = 7.91 \frac{X_p}{D} - 5.06 \left(\frac{X_p}{D} \right)^2$ (36) $\frac{d_s}{D} = 0.0342(\lambda) + 3.3437$	N/A	eq. 31 $0.3 \leq \lambda \leq 2.5$ eq. 32 $2.5 < \lambda < 3.0$ eq. 33 $3.0 < \lambda < 21.0$ eq. 35 $\lambda < 21.0$ eq. 36 $\lambda \geq 21.0$
	(34) $\lambda = \frac{NmV^2 10^{-6}}{D^3 f_c'}$			

Table 1 (concluded).

Model	Penetration depth (X_p)	Scabbing thickness (d_s)	Perforation thickness (d_p)	Application range	
Hughes	(37) $\frac{X_p}{D} = \frac{0.19N\lambda}{S}$	(40) $\begin{cases} \frac{d_s}{D} = 5.0 \frac{X_p}{D} & \frac{X_p}{D} \leq 7.0 \\ \frac{d_s}{D} = 1.74 \frac{X_p}{D} + 2.3 & \frac{X_p}{D} > 7.0 \end{cases}$	(41) $\begin{cases} \frac{d_p}{D} = 3.6 \frac{X_p}{D} & \frac{X_p}{D} \leq 7.0 \\ \frac{d_p}{D} = 1.58 \frac{X_p}{D} + 1.4 & \frac{X_p}{D} > 7.0 \end{cases}$	Conservative for:	
	(38) $S = 1.0 + \ln(1.0 + 0.03\lambda)$				$\begin{cases} \lambda < 40.0 \\ \frac{d_p}{D} < 3.5 \\ \frac{d_s}{D} < 3.5 \end{cases}$
	(39) $\lambda = 10^{-6} \frac{mV^2}{D^3 f_t'}$				
Riera	(42) $\lambda = \frac{\pi}{2} \left(\beta_1 \left(\frac{X_p}{D} \right) - \alpha_1 + \frac{L\alpha_2}{2D} \right)$	N/A	(46) $\begin{cases} \lambda = 30.97 \left(\frac{d_p}{D} \right) - \theta & \lambda \leq 30 \\ \frac{d_p}{D} = 3.31 + 0.0323(\lambda) & \lambda > 30 \end{cases}$	Without limitation	
	(43) $\alpha_1 = \beta_2 \frac{1 - \exp\left(-\frac{cX_p}{D}\right)}{c}$				
	(44) $\alpha_2 = \beta_1 - \beta_2 \exp\left(-\frac{cX_p}{D}\right)$		(47) $\theta = 103 \left[1 - \exp\left(-\frac{0.3d_p}{D}\right) \right]$		
	(45) $\lambda = 10^{-6} \frac{NmV^2}{2\pi D^3 f_t'}$				

Table 2. Notation, description, and unit of the terms used in a typical impact problem.

Parameter type	Notation	Description	Unit
Target response	X_p	Penetration depth	m
	d_p	Perforation thickness	m
	d_s	Scabbing thickness	m
Target properties	h	Thickness	m
	f_c^c	Concrete compressive strength	MPa
	f_t	Concrete tensile strength	MPa
	ρ	Concrete density	kg/m ³
	K	Concrete penetrability factor	—
	r	Ratio between in-plane steel mass and concrete volume	kg/m ³
	a	Half of concrete aggregate size	m
Missile properties	S	Dynamic increase factor	—
	V	Initial velocity	m/s
	W	Weight	N
	m	Mass	kg
	L	Length	m
	D	Diameter	m
	A_p	Weight per unit projected area	N/m ²
	N	Shape factor	—
General coefficients	E	Modulus of elasticity of missile	MPa
	E_m	Modulus of elasticity of steel	MPa
$\lambda, \beta_1, \beta_2, \alpha_1, \alpha_2, \theta, c$			—

dynamic increase factor (S). Riera (1989) developed another model for predicting the penetration depth by comparing the initial kinetic energy of the missile to the work performed during the penetration process. The formulation of the model was based on two assumptions: (1) the missile has a rigid-perfectly plastic behaviour, and (2) as the penetration depth increases, the resistance of the target increases monotonically until it reaches a limiting value. To consider soft missile impacts, the ratio of the missile length to diameter was included in the model. Unlike most other models, both the Hughes and Riera models use the tensile strength of concrete instead of the compressive strength to calculate the penetration depth.

With the previously mentioned models (except the Riera model), the relationship between the missile velocity and the perforation thickness is expressed in terms of the penetration depth. In 1968, the Ballistic Research Laboratory (BRL) proposed a formula to directly calculate the perforation thickness independently of the penetration depth (Gwaltney 1968). Later, Linderman et al. (1974) used the BRL formula and suggested a relationship for the scabbing thickness. Rotz (1976) from Bechtel Power Corporation proposed another relationship, known as the Bechtel formula, to estimate the scabbing thickness using more recent test data. Both the BRL and Bechtel formulae have no limitations in terms of application range. Berriaud et al. (1978) refined the BRL formula based on a series of impact tests carried out by the Commissariat à l'Énergie Atomique (CEA) – Electricité de France (EDF) and suggested a new relationship for perforation thickness known as the CEA-EDF formula. Later, Berriaud et al. (1982) modified this formula to take into account the influence of in-plane reinforcement ratio (r). Chang (1981) used Bayesian statistics and principles of mechanics to derive a new set of equations for scabbing and perforation thickness. With all the above-mentioned models, the perforation thickness can be predicted directly from the properties of the missile and target without the need to estimate the penetration depth.

3. Comparison of existing models against laboratory tests

To evaluate the accuracy of the existing models, a dataset of 95 impact tests reported in the literature was compiled. The

majority of the tests were obtained from a large experimental campaign conducted by CEA and EDF. Thirty-three of the tests were taken from Berriaud et al. (1978); 37 from Berriaud et al. (1982); 22 from Berriaud et al. (1979); and 3 from Vepsä et al. (2011) and Orbovic and Blahoianu (2011). The range of properties of the missiles and targets used in the compiled dataset is given in Table 3. The properties and parameters of the tests are wide ranging, meaning that the compiled dataset can be a good indication of the performance of numerical models. For more information on the compiled dataset, including the distribution of the target and missile properties, refer to Lulec (2017).

It should be noted that the dataset only includes the impact tests in which relatively large missiles (i.e., missile diameter is larger than 0.05 m) with initial velocities lower than 333 m/s were used. Other impact tests in which specimens were subjected to bullet-size penetrators with high velocities were not included in the dataset (e.g., Jinzhu et al. 2013). The damage mechanisms of these specimens are substantially different from those tested under larger-sized missiles with lower velocities. Additionally, the in-plane reinforcement in the test specimens considered was symmetrical about orthogonal directions. Specimens with non-symmetrical in-plane reinforcement were not considered in this study.

The performance evaluation was conducted based on the ability of the models to predict the perforation velocities of the impact tests. As previously defined, perforation velocity is the minimum velocity required for the missile to perforate the target. The perforation velocities were calculated by equating perforation thickness to the specimen depth and solving the equations presented in Table 1 for the missile striking velocity. The calculations were only performed for the missile tests within the applicability limits of each model. Figure 2 demonstrates the applicability rate and the correlation between the calculated and experimental velocity values (V_{exp} and V_{calc}) for each model. It also shows statistical parameters for the ratio of the calculated to experimental perforation velocities including the mean, coefficient of variation (CV), coefficient of determination (R^2), and root mean square (RMS) error.

A comparison of the results, presented in Fig. 2, shows that the predicted perforation velocity greatly depends on the selected

Table 3. Range of properties of missiles and targets used in dataset.

Parameter	Unit	Test series			
		Berriaud et al.			Vepsä et al. (2011); Orbovic and Blahoianu (2011)
		(1978)	(1979)	(1982)	
Number of specimens	—	33	22	37	3
Target thickness (h)	m	0.104–0.600	0.260–0.300	0.156–0.260	0.250
Concrete comp. strength (f'_c)	MPa	33.5–50.5	29.0–78.5	31.6–60.2	50.3–60.0
Shear reinf. ratio (ρ_v)	%	0–0.529	0–0.195	0–0.529	0–1.460
In-plane reinf. ratio - tension side (ρ_s)	%	0–1.608	0–0.967	0–1.510	0.698
Missile mass (m)	kg	30–303	53–315	7–252	47–48
Missile diameter (D)	m	0.100–0.305	0.100–0.300	0.050–0.250	0.168
Missile initial velocity (V)	m/s	21.9–216.0	18.8–144.0	12.5–333.0	110.0–144.0

model. In general, as the velocity required for perforation increased, the accuracy of the models diminished. Thus, caution must be taken when applying the models to thick or highly reinforced concrete panels, which have high resistance against missile perforation. In addition, models that expressed the relationship for the perforation thickness and velocity independently of the penetration depth had better performance (e.g., Chang, CEA-EDF, and Riera models). The reason is that equations for the penetration depth were derived based on the assumption of semi-infinite targets and may not be applicable to plate or shell elements with limited thickness. In the following section, the performance of each model is discussed in detail.

For both the Modified Petry and BRL models, no limitations were defined for their application to impact tests (i.e., applicability rate of 100%). However, perforation velocities predicted by both models did not correlate well with the experimental values. The relationship between the calculated and experimental velocities had coefficients of determination (R^2) of 0.73 and 0.83 for the Modified Petry and BRL models, respectively. Although both models performed well for specimens with perforation velocities less than 200 m/s, beyond this velocity the correlation between the calculated and experimental values quickly diminished. Additionally, both models overestimated perforation velocities for most of the tests. The ratio of the calculated to measured velocities had a mean of 1.62 for the Modified Petry model and 1.73 for the BRL model. This means that for many of the specimens where perforation of the target was observed in the test, the models predicted no perforation and estimated that larger velocities were required to cause the perforation. Correctly predicting whether a missile perforates a structural element or not is critically important; perforation can cause significant damage not only to the structural system but also to the equipment and people inside the structure.

Unlike the Modified Petry and BRL models, the NDRC model underestimated velocities for most of the tests resulting in a mean of 0.88 and the coefficient of variation (CV) of 33.9% for the ratio of the calculated to measured velocities. Thus, the model yielded conservative results for the majority of the impact tests. Even though the correlation between the calculated and experimental perforation velocities was relatively low, with its high applicability rate (98%) and conservative predictions, the NDRC model can be a good choice for design purposes.

The ACE model was only applicable to four tests, which makes it difficult to evaluate the performance of the model. The Kar model is mainly a combination of the ACE and NDRC models, except for the addition of the nose factor. However, this modification did not yield significant changes to the results. The results obtained from the Kar model were similar to those obtained from the NDRC model and not the ACE model. This is mainly due to the high applicability ratio of the NDRC model compared to

the ACE model (98% versus 4%). All three models yielded conservative predictions.

The CEA-EDF model was one of the most accurate models examined when applied to this dataset, with a mean of 1.00 and CV of 8.9% for the ratio of the calculated to experimental velocities; as well, it returned a strong R^2 value of 0.96. One reason behind its high level of accuracy is that the relationship between the perforation velocity and thickness is solely expressed in terms of properties of the missile and target and not the penetration depth. With the modification for the reinforcement, the CEA-EDF (r) model became more conservative than the original model which resulted in a weaker correlation with the experimental results. Both models resulted in low applicability ratios (35% for the original model and 38% for the modified model).

The Riera and Chang models were among the more accurate models for this dataset. The Riera model resulted in a mean square root (RMS) error and R^2 of 25.87 m/s and 0.90, while the corresponding values for the Chang model were 18.90 m/s and 0.95, respectively. The RMS error values of the two models were among the lowest of all the models studied in this paper. This statistical parameter indicates how spread out the data are from the line of best fit. With both models, similar to the CEA-EDF model, the perforation velocity is calculated without using the penetration depth. Although the Riera model was applicable to all the tests, the ratio of the calculated to experimental velocities had a mean of 1.30, making it significantly unconservative. The Chang model had a better correlation between the calculated and experimental results with a mean and CV of 0.97 and 11.5%, respectively. However, this model was only applicable to 54% of the tests.

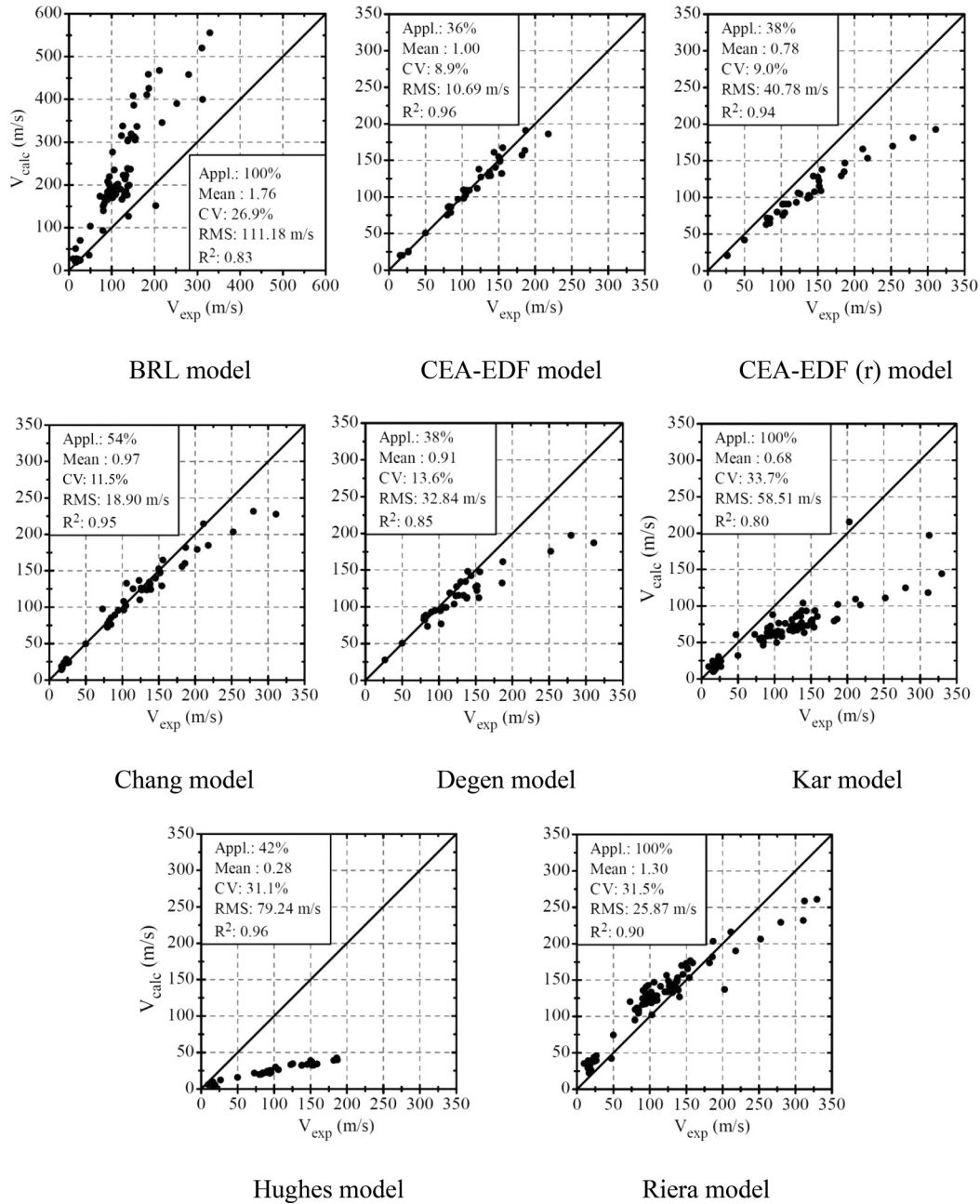
The ratio of the calculated to experimental velocities for the Hughes model had a mean of 0.28 and CV of 31.1% making it considerably less accurate compared to the rest of the models. However, the model indicated a high linear correlation ($R^2 = 0.96$) meaning that using a calibration factor the accuracy of the results can be significantly improved. In this study, the calibration factor was determined as 0.28, which is the mean of the ratio of the calculated to experimental velocities. Using this calibration factor, the RMS error value of the model can be reduced from 79.24 m/s to 18.42 m/s. Another major drawback of the model was its low applicability rate (42%).

The Degen model had a similar applicability rate as that for the Hughes model. However, the results of the Degen model were much more accurate with a mean of 0.91 and a CV of 13.6% for the ratio of the calculated to experimental velocities. The Bechtel and Halder models were not able to predict the perforation velocity as they do not have relationships for perforation thickness.

4. Formulation of the proposed model

Formulation of the proposed model comprised three main parts: the perforation energy (E_p), which defines a relationship for the perforation velocity; the perforation work (W_p), which is

Fig. 2. Comparison of calculated and experimental perforation velocities.



calculated based on the principle of work and the Modified Compression Field Theory (Vecchio and Collins 1986); and the deformation energy (E_d), which is estimated using experimental data reported from the literature. The relationship between these three components results in a semi-analytical model for calculating perforation velocity. Details of each component are presented in the following sections.

4.1. Perforation energy, E_p

According to Rotz (1976), the relation for the energy balance of a structural system subjected to impact loading can be presented as

$$(48) \quad E_i = E_p + E_r$$

where E_i , E_p , and E_r are the initial, perforation, and residual energies, respectively. This equation can be restated as

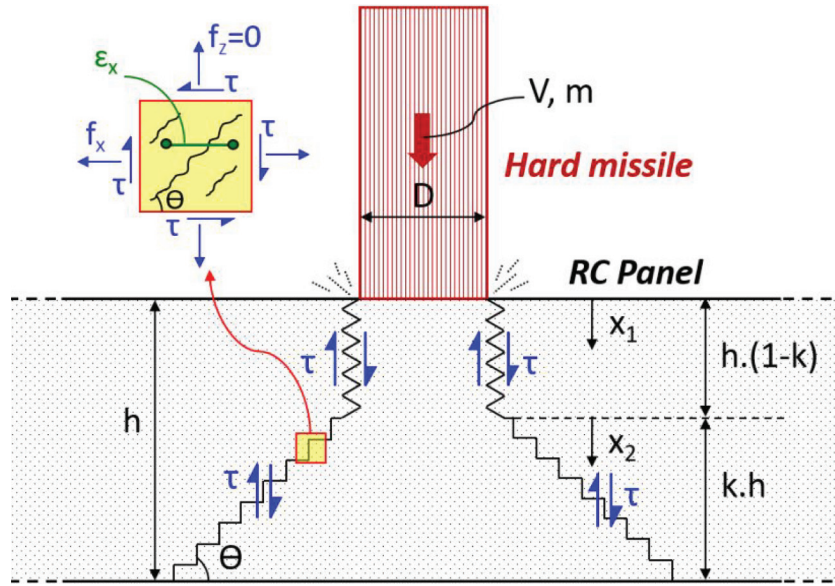
$$(49) \quad \frac{1}{2}mV^2 = E_p + \frac{1}{2}mV_r^2$$

where m , V , and V_r are the mass, striking velocity, and residual velocity of the missile, respectively. In the special case where the residual velocity is zero, the initial velocity will be equal to the perforation velocity, which is the minimum velocity required for perforation. In this case, the energy balance equation becomes

$$(50) \quad \frac{1}{2}mV_p^2 = E_p$$

Therefore, if the perforation energy is calculated, the perforation velocity can be determined.

Fig. 3. Plug formed in concrete target due to hard missile impact. [Colour online.]



4.2. Perforation work, W_p

There are several mechanisms that contribute to the energy dissipation of a missile impact including overall movement of the target, shear plugging, deformation of the missile, interface loads between the missile and target, ejecting particles, and losses due to heat transfer. For relatively thick RC panels subjected to hard missiles, shear plugging is considered one of the most significant controlling mechanisms. Figure 3 shows the shear plug formed due to the impact of a missile on an RC panel with a depth of h .

As observed in many experiments (e.g., Vepsä et al. 2011; Orbovic et al. 2009), the shear plug is initially in a cylindrical form; at some point, it expands forming a conical shape with a crack angle of θ . In Fig. 3, k is the ratio of the depth of the shear cone to the total depth of the target, and τ is the shear stress along the cracks.

The energy dissipation due to shear plugging can be estimated based on the principle of work-energy. According to this principle, the change in the kinetic energy of a system equals the work done by the resultant force acting on the system. In general, the work performed by a force, F , can be calculated as

$$(51) \quad \text{Work} = \int F(x) dx$$

where $F(x)$ is the force as a function of x which is the distance travelled due to F . This relation can be used to calculate the work performed, W_p , during the perforation process. Since the shape of the shear plug changes through the depth, the calculation of W_p is divided into two parts. The cylindrical part of the shear plug is calculated using the distance variable x_1 , while the conical part of shear plug is computed based on the distance variable x_2 . Using eq. 51 and the geometry of the shear plug presented in Fig. 3, the perforation work can be expressed as

$$(52) \quad W_p = \int_0^{h(1-k)} \tau \pi d [h(1-k) - x_1] dx_1 + \int_0^{kh} \tau \pi [d + 2x_2 \tan(90 - \theta)] [kh - x_2] dx_2$$

Solving the integrals results in the following equation:

$$(53) \quad W_p = \frac{\tau \pi d}{2} [h(1-k)]^2 + \tau \pi \left[\frac{d(kh)^2}{2} + \frac{(kh)^3}{3} \tan(90 - \theta) \right]$$

The unknown variables in this equation are the shear stress (τ), crack angle (θ), and k coefficient. The shear stress and crack angle are determined based on a procedure drawn from the Modified Compression Field Theory (MCFT) (Vecchio and Collins 1986). The MCFT is a well-recognized theoretical model for computing the nonlinear response of RC elements under general loading conditions, particularly shear loads. To calculate the shear stress required to cause the perforation, instead of the full stress-strain relationship of an element, only the shear strength of the section and the corresponding crack angle are needed. Using the full version of the MCFT to calculate the shear strength of a section is relatively complex and is not suitable for design procedures. Bentz and Collins (2006) developed a simplified version of the MCFT which can conveniently calculate the shear strength with nearly the same level of accuracy as the full model. Also, a practical version of the MCFT, known as the Sectional Design Method (SDM), is used for shear design provisions of CSA A23.3 (2014). In this study, a combination of these two methods was used to calculate the shear strength and crack direction in a practical and accurate manner.

Using equilibrium conditions, the simplified MCFT expresses the total shear stress of a section as a summation of the shear stress in the concrete and the shear stress in the transverse reinforcement:

$$(54) \quad \tau = \tau_c + \tau_s = \beta \sqrt{f'_c} + \rho_v f_y \cot \theta \leq 0.25 f'_c$$

where ρ_v and f_y are the ratio and yield strength of the shear reinforcement, β is a factor accounting for the shear resistance of cracked concrete, and θ is the angle of inclination of the diagonal compressive stresses (i.e., the crack angle). The equation assumes that the clamping stresses are negligible ($f_z = 0$) and that the shear reinforcement yields at failure. Bentz and Collins (2006) demonstrated that if the shear strength is below the $0.25 f'_c$ limit, the assumption that the shear reinforcement is yielding at failure is appropriate. The model uses the following simplified equations to estimate β and θ :

Can. J. Civ. Eng. Downloaded from cdnsciencepub.com by CARLETON UNIV on 03/15/21 For personal use only.

$$(55) \quad \beta = \frac{0.40}{1 + 1500x} \times \frac{1300}{1000 + s_{ze}}$$

$$(56) \quad \theta = 29^\circ + 7000\varepsilon_x$$

where ε_x is the in-plane strain at the mid-depth of the cross section and s_{ze} is the effective crack spacing parameter. Based on the SDM method, s_{ze} can be taken as 300 mm if the amount of shear reinforcement in the section is larger than $A_{v,min}$ expressed as

$$(57) \quad A_{v,min} = 0.06 \frac{\sqrt{f_c} b_w s}{f_y}$$

For members without minimum shear reinforcement, s_{ze} should be calculated using the following equation:

$$(58) \quad s_{ze} = \max\left(\frac{35s_z}{15 + a_g}, 0.85s_z\right)$$

where s_z is the crack spacing parameter and a_g is the aggregate size. s_z can be taken as the effective shear depth of the section (d_v) or the maximum spacing between layers of the in-plane reinforcement. The in-plane strain at the mid-depth of the section (ε_x) can be estimated from the applied forces to the section

$$(59) \quad \varepsilon_x = \frac{M_f/d_v + 0.5N_f + V_f}{2E_s A_s}$$

where M_f , N_f , and V_f are the applied bending moment, axial force, and shear force to the section, respectively. E_s and A_s are the modulus of elasticity of steel and the cross-sectional area of in-plane reinforcement on the flexural tension side of the section, respectively. To calculate the shear strength of a member subjected to pure shear, N_f and M_f are taken as zero. Dividing both the numerator and denominator of eq. 59 by $b_w d_v$ yields

$$(60) \quad \varepsilon_x = \frac{\tau}{2E_s \rho_s}$$

where ρ_s is the in-plane reinforcement ratio on the tension side. Since the in-plane strain (ε_x) is a function of the shear stress (τ), an iterative procedure is required to determine these two parameters. The steps required to complete this procedure are demonstrated in Fig. 4. The procedure is repeated until the in-plane strain converges within a predefined error limit. After convergence is achieved, the adequacy of the in-plane reinforcement to

transmit additional stresses caused by shear across the crack needs to be checked:

$$(61) \quad \rho_x f_y \geq [\tau - 0.5\rho_w f_y \cot(\theta)] \cot(\theta)$$

If eq. 61 is not satisfied, ε_x should be increased until the equation is satisfied. After this final check, the process is completed, and the final values of τ and θ are obtained.

4.3. Deformation energy, E_d

The perforation work calculated in Section 4.2 considers the energy dissipation due to the shear plugging mechanism during an impact load. To account for other mechanisms (e.g., target and missile deformations, ejecting particles, etc.) contributing to the energy dissipation, an additional energy term needs to be defined. In this study, this additional term is named deformation energy (E_d) and is calculated by subtracting the total perforation energy from the perforation work due to the shear plugging

$$(62) \quad E_d = E_p - W_p$$

Using data reported from the missile tests, the following equation is proposed to estimate the deformation energy:

$$(63) \quad E_d = c_1 \left[\frac{d^3 f_t h^5}{m} \right]^{c_2}$$

where c_1 and c_2 are coefficients calculated according to a statistical analysis which minimized the root mean square of the error between the perforation energy values estimated from the initial and residual velocities reported from tests and the summation of the perforation work and deformation energy values calculated from eqs. 53 and 63. Additionally, using a similar statistical procedure, the ratio of the height of the conical shear plug to the target thickness (k) is found to be 0.65. Substituting the calculated values into eq. 62 yields

$$(64) \quad \frac{1}{2} m V_p^2 = \frac{\tau \pi d}{2} [0.35h]^2 + \tau \pi \left[\frac{d(0.65h)^2}{2} + \frac{(0.65h)^3}{3} \tan(90 - \theta) \right] + 660000 \left[\frac{d^3 f_t h^5}{m} \right]^{0.56}$$

where τ and f_t are in Pascals, h and d are in metres, θ is in degrees, and m is in kilograms. Solving this equation for V_p and rearranging the coefficients to convert τ and f_t into megapascals yields:

$$(65) \quad V_p = \sqrt{2 \times 10^6 \frac{\tau \pi}{m} \left[\frac{0.55d(h)^2}{2} + \frac{(0.65h)^3}{3} \tan(90 - \theta) \right] + \frac{3 \times 10^9}{m} \left[\frac{d^3 f_t h^5}{Nm} \right]^{0.56}}$$

To account for the nose shape of the missile, the nose shape factor (N) was included in this equation. N is 1.0 for flat noses, and can be calculated for conical and blunt noses according to the following relationships proposed by Chen and Li (2002):

$$(66) \quad N = \begin{cases} \frac{1}{1 + 4(S/D)^2} & \text{Conical nose} \\ 1 - \frac{1}{8(S/D)^2} & \text{Blunt nose} \end{cases}$$

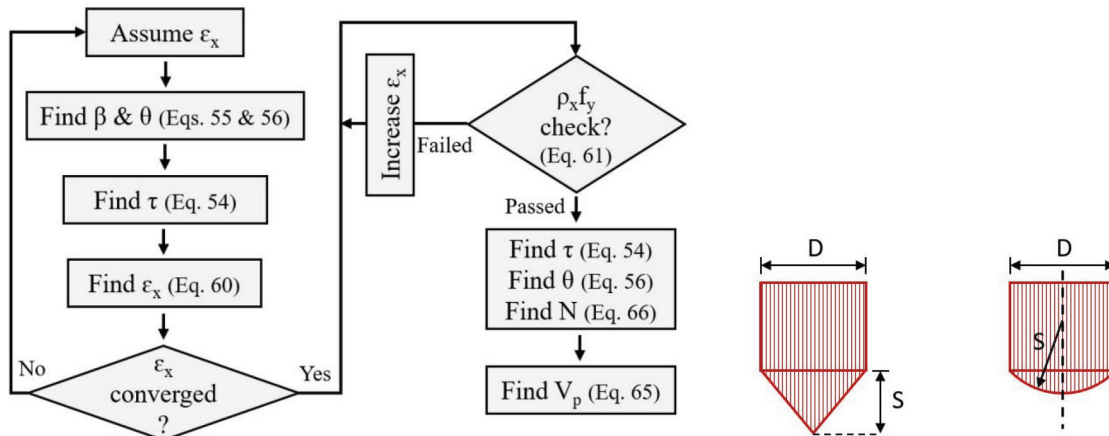
where D is the diameter of the missile and S , depending on the nose shape, is the distance between the tip and base of the nose or is the radius of the missile nose (see Fig. 4).

It should be noted that the proposed model does not explicitly take into account dynamic effects on material properties (also known as strain rate effects) because determining these effects requires knowing the missile velocity. Instead, the dynamic effects are implicitly included in the model through the c_1 and c_2 coefficients which were determined by statistical analysis of experimental results reported from the dataset.

5. Verification of the proposed model

The accuracy of the proposed model was evaluated against the previously mentioned compiled dataset. Out of the 95 missile tests, the model was not applicable to the 5 tests that did not contain any in-plane reinforcement and experienced a different

Fig. 4. Algorithm of the proposed model (left) and definitions of D and S for nose factor (right). [Colour online.]



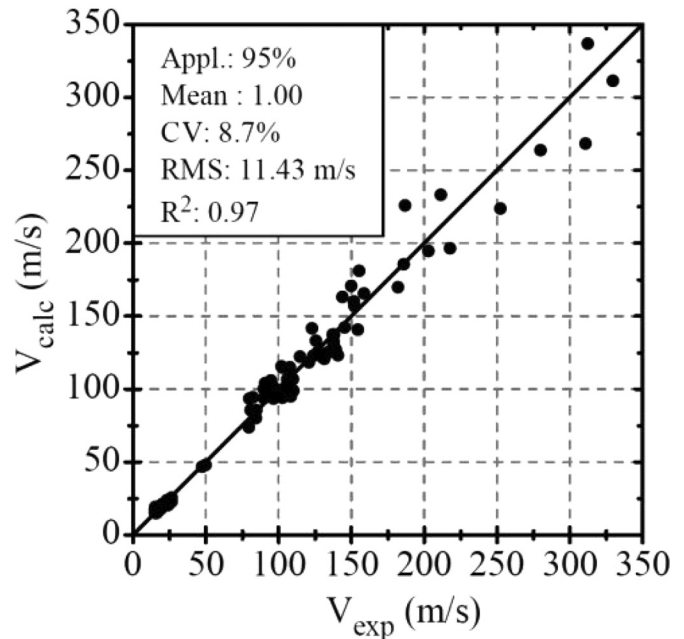
type of failure compared to the rest of the dataset. For the remaining 90 tests in which the failure was governed by shear plugging, the calculated and experimental perforation velocities (V_{calc} and V_{exp}) are compared and presented in Fig. 5. The mean and coefficient of variation for the ratio of the predicted to measured velocities are 1.00 and 8.7%, respectively. Additionally, the coefficient of determination and the root mean square error found to be 0.97 and 11.43 m/s, respectively. Based on these statistical parameters, it can be concluded that there is a high correlation between the predicted and experimental results.

In addition to comparison of the proposed model with experimental data, its performance against other commonly used models was evaluated. The applicability rate as well as the mean and CV of the ratio of the predicted to measured perforation velocities for each model are shown in Figs. 6–8. For comparisons of other statistical parameters (RMS error and R^2) between different models, refer to Lulec (2017).

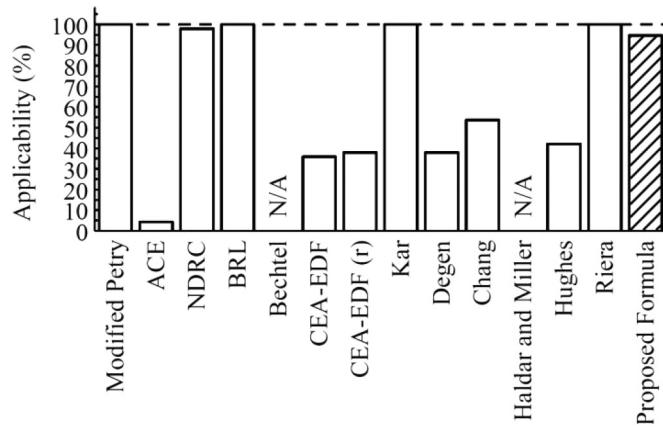
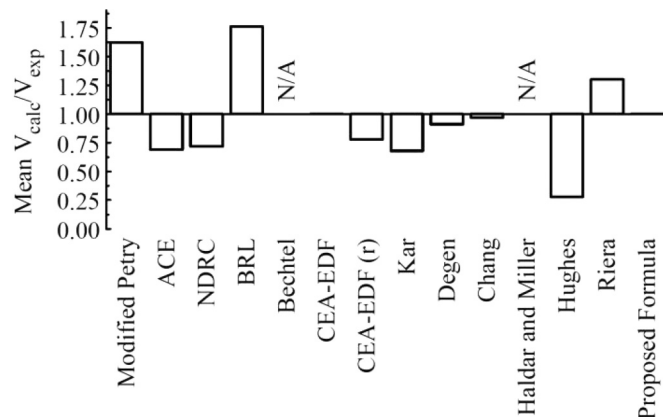
In terms of the applicability rate, the Modified Petry, BRL, Kar, and Riera models were applicable to all the tests in this dataset. However, no limitations were defined for these models, which raises concerns about their accuracy. With an applicability rate of 95%, the proposed model was among the most encompassing in terms of range. However, the model was not applicable to specimens that did not contain any in-plane reinforcement. For these specimens, eq. 60 results in an infinite value for the in-plane strain which consequently leads to inaccurate values for the shear stress and crack angle. This is because the model calculates the flexural capacity of a section solely based on the amount of in-plane reinforcement neglecting the contribution of concrete on the tension side of the section. Further work is needed to extend the model to calculate the flexural and shear capacity of plain concrete sections according to the cracking strength of concrete.

The most accurate models can be judged according to the mean value and CV of the ratio of the calculated to measured velocities as well as the RMS error values. According to these three metrics, the CEA-EDF model (mean: 1.00, CV: 8.9%, RMS error: 10.69 m/s), the Chang model (mean: 0.97, CV: 11.5%, RMS error: 18.90 m/s), and the proposed model (mean: 1.00, CV: 8.7%, RMS error: 11.43 m/s) had perforation velocity predictions closest to the experiments. Recall that the applicability rate of the CEA-EDF and Chang models for this dataset were 36% and 54%, respectively. Thus, the proposed model has the highest applicability amongst the models that exhibited high accuracy, as well as being more rational rather than fully-empirical in terms of the parameters considered. Furthermore, unlike most existing models

Fig. 5. Correlation between predicted (proposed model) and experimental perforation velocities.



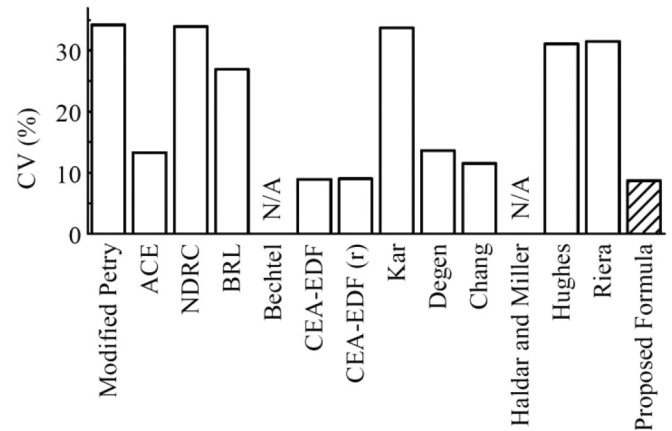
which had difficulties in capturing the response of specimens with high perforation velocities, the proposed model was able to calculate the perforation velocity of these specimens with an acceptable level of accuracy. Most importantly, none of the models reviewed in this study were able to explicitly take into account the influence of shear reinforcement. The proposed model provided a comprehensive rational method for calculating the contribution of shear reinforcement. It should be noted that in the proposed model, the contributions to energy dissipation of mechanisms other than shear plugging are calculated based on the statistical analysis of the results of impact tests with missile diameters larger than 0.05 m and initial velocities lower than 333 m/s. The application of the model to other impact tests with smaller missile diameters or higher initial velocities has not been verified. In particular, the model may not be applicable to impact tests with bullet-size penetrators with high velocities where the failure mode is different than shear plugging.

Fig. 6. Comparison of models in terms of applicability rate.**Fig. 7.** Comparison of models in terms of mean value of $V_{\text{calc}}/V_{\text{exp}}$.

6. Conclusions

A semi-analytical model for the calculation of perforation velocity of a hard missile impact on a reinforced concrete wall panel was developed. The model uses the principle of work-energy to calculate the energy dissipation due to shear plug movement as well as overall target movement during the perforation process. The angle of the shear plug and the shear strength of the target were calculated according to the MCFT theory, which enables inclusion of the influence of in-plane and shear reinforcement. The model was validated with 95 tests from different sources in the literature, and its performance was compared against 13 commonly used models. The comparison of results yielded the following conclusions:

1. Most of the empirical models examined in this study could not accurately calculate the perforation velocities for specimens within the broad dataset compiled. The ones that performed well had a limited applicability range.
2. In general, as the velocity required for perforation increased, the accuracy of the models diminished. Thus, caution must be taken when applying the empirical models to thick or highly reinforced concrete panels, which have high resistance against missile perforation.
3. Models that expressed the relationship for the perforation thickness and perforation velocity independent of the penetra-

Fig. 8. Comparison of models in terms of CV of $V_{\text{calc}}/V_{\text{exp}}$.

tion depth had better performance. Also, neglecting the influence of in-plane or shear reinforcement detrimentally influenced the accuracy of the models.

4. The proposed model was able to provide accurate calculations of perforation velocities for the compiled dataset. The ratio of the predicted to experimental values had a mean of 1.00 and a coefficient of variation of 8.7%. The high accuracy of the model is mainly attributed to its detailed rational procedure for taking into account the shear effects.
5. Although the proposed model showed high levels of accuracy and applicability for the examined dataset, it should be noted that some of the coefficients used in the model were obtained from the same series of tests. Therefore, it is important to further verify the model with other missile tests in the future.
6. The proposed model was not applicable to the 5 of 95 missile tests that did not contain any in-plane reinforcement. For these specimens, the shear strength and crack angle could not be accurately determined. Work is required to extend the application of the model to these types of specimens.
7. The model has the potential to be extended to other types of reinforcements such as prestressed or fibre reinforced concrete. It is worth noting that the MCFT is capable of calculating the shear strength and crack angle for these types of reinforcements (e.g. Lee et al. 2016).

Acknowledgements

Financial support provided by the Natural Sciences and Engineering Research Council of Canada (NSERC) and the Morrison Hershfield engineering firm is gratefully acknowledged.

References

- Amirikian, A. 1950. Design of protective structures. Report NT-3726. Bureau of Yards and Docks, Department of the Navy, Washington, D.C.
- Army Corps of Engineers (ACE). 1946. Fundamentals of protective design. Report AT120 AT1207821, Army Corps of Engineers, Office of the Chief of Engineers, U.S.A.
- Bentz, E.C., and Collins, M.P. 2006. Development of the 2004 Canadian Standards Association (CSA) A23.3 shear provisions for reinforced concrete. *Canadian Journal of Civil Engineering*, 33(5): 521–534. doi:10.1139/106-005.
- Berriaud, C., Verpeaux, P., Hoffmann, A., Jamet, P., and Avet-Flancard, R. 1979. Test and calculation of the local behaviour of concrete structures under missile impact. 5th Int. Conf. on Structural Mechanics in Reactor Technology (SMIRT5), Berlin, Germany.
- Berriaud, C., Verpeaux, P., Jamet, P., Avet-Flancard, R., and Perrot, J. 1982. Concrete wall perforation by rigid missile. In RILEM Conference, Symposium on Concrete Structures under Impact and Impulsive Loading, Berlin, Germany.

- Berriaud, C., Sokolovsky, A., Gueraud, R., Dulac, J., and Labrot, R. 1978. Local behavior of RC walls under missile impact. *Nuclear Engineering and Design*, **45**(2): 457–469. doi:10.1016/0029-5493(78)90235-2.
- Chang, W.S. 1981. Impact of solid missiles on concrete barriers. *ASCE Journal of the Structural Division*, **107**(2): 257–271.
- Chelapati, C.V., Kennedy, R.P., and Wall, I.B. 1972. Probabilistic assessment of aircraft hazard for nuclear power plants. *Nuclear Engineering and Design*, **19**(2): 333–364. doi:10.1016/0029-5493(72)90136-7.
- Chen, X.W., and Li, Q.M. 2002. Deep penetration of a non-deformable projectile with different geometrical characteristics. *International Journal of Impact Engineering*, **27**(6): 619–637. doi:10.1016/S0734-743X(02)00005-2.
- CSA A23.3. 2014. Design of concrete structures (CSA A23.3-14). Canadian Standards Association, Mississauga, Canada.
- Degen, P.P. 1980. Perforation of reinforced concrete slabs by rigid missiles. *Proceedings of the American Society of Civil Engineers, ASCE Journal of the Structural Division*, **106**: 1623–1642.
- Gwaltney, R. 1968. Missile generation and protection in light-water-cooled power reaction plants. Report ORNL NSIC-22, Oak Ridge National Laboratory, Oak Ridge, Tenn.
- Haldar, A., and Hamieh, H.A. 1984. Local effects of solid missiles on concrete structures. *Journal of Structural Engineering, ASCE*, **110**(5): 948–960. doi:10.1061/(ASCE)0733-9445(1984)110:5(948).
- Haldar, A., and Miller, F.J. 1982. Penetration depth in concrete for nondeformable missiles. *Nuclear Engineering and Design*, **71**(1): 79–88. doi:10.1016/0029-5493(82)90171-6.
- Hughes, G. 1984. Hard missile impact on reinforced concrete. *Nuclear Engineering and Design*, **77**(1): 23–35. doi:10.1016/0029-5493(84)90058-X.
- Jinzhua, L., Zhongjie, L., Hongsong, Z., and Fenglei, H. 2013. Perforation experiments of concrete targets with residual velocity measurements. *International Journal of Impact Engineering*, **57**: 1–6. doi:10.1016/j.ijimpeng.2013.01.007.
- Kar, A.K. 1978. Local effects of tornado-generated missiles. *Journal of the Structural Division, ASCE*, **104**(5): 809–816.
- Kennedy, R.P. 1976. A review of procedures for the analysis and design of concrete structures to resist missile impact effects. *Nuclear Engineering and Design*, **37**(2): 183–203. doi:10.1016/0029-5493(76)90015-7.
- Lee, S.C., Cho, J.Y., and Vecchio, F.J. 2016. Analysis of steel fiber-reinforced concrete elements subjected to shear. *ACI Structural Journal*, **113**(2): 275–285. doi:10.14359/51688474.
- Linderman, R.B., Rotz, J.V., and Yeh, G.C.K. 1974. Design of structures for missile impact. Report BC-TOP-9A, Bechtel Power Corporation, Calif.
- Lulec, A. 2017. Simplified analytical tools for impact and impulsive loading analysis of reinforced concrete structures. Ph.D. thesis, University of Toronto, Ont., Canada.
- National Defense Research Committee (NDRC). 1946. Effects of impact and explosion. Summary Technical Report of Division 2, National Defense Research Committee, Washington, D.C.
- Orbovic, N., and Blahoianu, A. 2011. Tests on concrete slabs under hard missile impact to evaluate the influence of transverse reinforcement and pre-stressing on perforation velocity. *In The 21st International Conference on Structural Mechanics in Reactor Technology (SMIRT21)*, New Delhi, India.
- Orbovic, N., Elgohary, M., Lee, N., and Blahoianu, A. 2009. Tests on RC slabs with pre-stressing and with transverse reinforcement under impact loading. *In The 20th International Conference on Structural Mechanics in Reactor Technology (SMIRT20)*, Espoo, Finland.
- Riera, J.D. 1989. Penetration, scabbing and perforation of concrete structures hit by solid missiles. *Nuclear Engineering and Design*, **115**(1): 121–131. doi:10.1016/0029-5493(89)90265-3.
- Rotz, J.V. 1976. Evaluation of tornado missile impact effects on structures. *In Proceedings of a Symposium on Tornadoes, Assessment of Knowledge and Implications for Man*, Lubbock, Texas.
- Samuely, F.J., and Hamann, C.W. 1939. Civil protection. The Architectural Press, London, U.K.
- Vecchio, F.J., and Collins, M.P. 1986. The modified compression-field theory for reinforced concrete elements subjected to shear. *ACI Journal*, **83**(2): 219–231.
- Vepsä, A., Saarenheimo, A., Tarallo, F., Rambach, J.M., and Orbovic, N. 2011. IRIS-2010- Part II: experimental data. *In The 21st International Conference on Structural Mechanics in Reactor Technology (SMIRT21)*, New Delhi, India.